Thermal effects on plastic instability of materials

Dierick, M.C.A.

Award date:
1987

Graduation research project report:

Thermal effects on plastic instability of materials

M.C.A. Dierick

October 1987
VF code C2 WPA 0492

Opmerkingen:

→ o.a. p. 26 bovenaan: wat ik mis is een verhalende/fysische interpretatie van het fenomeen therm. instabiliteit, en wel als element in de verzameling van instabiliteiten. (Zie ook p 29 midden in)

→ o.a. p. 25! Waarom niet eens met andere vloeikrommen van kunststof iets geprobeerd. Voorb: zie p44/45 → kunststoffen hebben al een vloeispanningsinstabiliteit!

→ kun je de FLP" verklaren? (Zie p40 bovenaan en introductie of 6.4 / p 15)
(in Schaap 12" verschil tussen b'n op p40, en a7 op p36 lijkt)

→ p. 29 onwetenschappelijke opmerking! Waarom? (volgens Popper bij v.)

→ p12: Waarom vloeipunktie niet genummerd? (zie ook p 36)

→ symbool A " → zie p. 6. opm. (zie ook p 39)

→ p. 48 experimenten: situatieschets bij foto?

PREFACE

This report contains the results of the graduation research project I carried out at the Division of Production Technology of the Department of Mechanical Engineering of the Eindhoven University of Technology.
Within the Division of Production Technology, the research group of prof. ir. J.A.G. Kals specializes in the behavior of materials during manufacturing processes. Instability phenomena encountered during plastic deformation of materials are one topic of interest in this field. In this report, an attempt is made to develop a comprehensive theory of such instability phenomena as they occur during cold working of materials, with the object of providing a fairly easy-to-use set of instability criteria for use by those designing products and production processes.
Carrying out a graduation research project is never the work of only one person. In particular, the comments and insights of prof. ir. J.A.G. Kals and dr. ir. J.H. Dautzenberg are appreciated. In addition, I would like to thank J. Boekholt of the Department of Chemical Technology for his help in carrying out the experiments. Lastly, I would like to thank my parents, T.M. Dierick and P.G. Dierick-van Knippenberg, and ms. J.B.M. Schoolkate, without whose understanding and support the completion of this graduation research project would not have been possible.

Maurice Dierick
Eindhoven, October 1987

There's a lone soldier on the cross
Smoke pouring out of a boxcar door
You didn't know it
You didn't think it could be done
In the final end he won the war
After losing every battle

Bob Dylan, The Idiot Wind

There's room at the top
They are telling you still
But first you must learn
How to smile as you kill
If you want to be
Like the folks on the hill

John Lennon, Working Class Hero

ABSTRACT

Materials undergoing plastic deformation fail by fracture in a field of homogeneous deformation or by fracture preceded by the concentration of deformation in a very small area: flow localization.
Results of researchers in the field of flow localization, influenced or caused by thermal effects, during plastic deformation at room temperature show that, although it is possible to calculate the strain at which such flow localization initiates and to give a description of the localization process after it has initiated, there is still no comprehensive theory of thermally influenced flow localization. Therefore it is attempted to derive such a theory, based on research by Kals and Semiatin et al. This theory, which includes both the initiation of localization and a description of its subsequent progress, is tested by carrying out tensile tests at high strain rates and applying it to data from the literature. The conclusion is that a general theory of flow localization has been derived and that such a theory can be used to predict maximum allowable strains for a number of manufacturing processes.

SAMENVATTING

Materialen die plastisch vervormd worden, kunnen op twee manieren breken: er kan breuk optreden voorafgegaan door volledig homogene deformatie, of er kan breuk optreden voorafgegaan door zeer sterk op een plaats geconcentreerde deformatie, ofwel gelokaliseerde deformatie.
Uit de literatuur op het gebied van thermisch beinvloede gelokaliseerde deformatie tijdens het plastisch bewerken van materialen op kamertemperatuur kan geconcludeerd worden dat, hoewel het mogelijk is om het begin van gelokaliseerde deformatie te voorspellen en een beschrijving te geven van de voortgang ervan, er nog steeds geen algemene theorie over dit verschijnsel bestaat. In dit verslag wordt geprobeerd een dergelijke theorie af te leiden op basis van onderzoek verricht door Kals en Semiatin en medewerkers. Deze theorie, waarmee zowel het ontstaan als het voortschrijden van gelokaliseerde deformatie wordt beschreven, wordt vervolgens beproefd m.b.v hoge-snelheids trekproeven en vergelijkend literatuuronderzoek. De conclusie luidt dat een algemene theorie van gelokaliseerde deformatie is afgeleid en dat m.b.v. deze theorie maximaal toelaatbare rekken voor een aantal bewerkingsprocessen kunnen worden afgeleid.

LIST OF SYMBOLS AND ABBREVIATIONS

ϱ [kg * m^{-3}]	specific weight
c [J * kg^{-1} * K^{-1}]	specific heat
n [-]	strain hardening exponent
m [-]	strain rate hardening exponent
T [K]	temperature
h(T) [-]	function of temperature
α [-]	fraction of heat retained
$\bar{\varepsilon}$ [-]	effective strain
ε [-]	principal strain
A [-]	engineering strain
$\dot{\varepsilon}$ [s^{-1}]	effective strain rate
$\bar{\sigma}$ [N * mm^{-2}]	effective stress
σ [N * mm^{-2}]	principal stress
K [N * mm^{-2} * s^{-1}]	material constant
i [-]	stress path
$\frac{\partial \sigma}{\partial T}$ [N * mm^{-2} * K^{-1}]	temperature dependence of stress
FLP [-]	Flow Localization Parameter
s [mm]	thickness of a blank
FLITE	Flow Localization Influenced by Thermal Effects

CONTENTS

1. INTRODUCTION

The study of failure modes of materials during processing and service is an important aspect of mechanical engineering, since understanding of the failure modes of materials can lead to improvements in the design and efficiency of production processes.

When studying the failure modes of materials, it should be noted that there are essentially two failure mechanisms **[26]**: fracture controlled failure and flow localization controlled failure. In the former case, failure occurs by fracture in a relatively homogeneous field of deformation, whereas it occurs in a region where flow has localized prior to fracture in the latter case. It is this last mechanism in which we are interested in this study. More specifically, we are interested in flow localization caused or influenced by thermal effects, such as (quasi-) adiabatic deformation heating. Common names for this phenomenon are adiabatic shear, catastrophic shear, thermo-plastic shear instability, and several others of this type. Since these cannot be used when one is speaking in general terms of thermally influenced flow localization, the acronym FLITE, for 'Flow Localization Influenced by Thermal Effects', will be used to denominate the phenomenon in this report. The object of this study is to formulate a theory of FLITE during plastic deformation of materials at room temperature, but without including the metallurgical aspects of FLITE.

As a starting point for the formulation of such a theory, a literature survey was carried out, the results of which were combined with Kals' instability analyses **[1]** to create a general theory of FLITE, which, after being tested experimentally, can be used to derive design criteria for a range of manufacturing processes.

2. LITERATURE SURVEY

2.1. Introduction

FLITE was first observed by Zener and Hollomon [8] in 1944. They encountered it in very high-speed punching of steel. At these speeds, the deformation process becomes adiabatic, meaning that all plastic work is transformed locally into heat. The temperature rise associated with this transformation results in a decrease in flow stress (flow softening) which, if larger than the increase in flow stress due to the deformation (strain hardening) causes localized deformation, or FLITE.
It was not until 1964 that the first mathematical models of FLITE were presented by Recht [5] and Chin et al. [28, 29]. From 1964 on, numerous articles on FLITE have appeared.
FLITE research can be divided in two parts:

- the mechanical aspects associated with FLITE, i.e. material parameters of importance and critical strains.
- the metallurgical aspects associated with FLITE, i.e. the structure of the zone of localized deformation, the influence of initial material defects on localization.

In this report, we are interested in the mechanical aspects of FLITE. The metallurgical aspects of FLITE will be discussed only if necessary.

2.2. FLITE modeling

There are principally two ways of modeling FLITE. The first method is based on thermodynamics, the second on plasticity theory. Since the first method is much more complex and does not yield appreciably different results, it will not be discussed further. For examples of this method, see the papers of Merzer [15], Bai [24, 40] and Wright and Batra [45].
The second method is based on the assumption that there is an equation of state relating stress, strain, strain rate and temperature. A criterion for the initiation of FLITE is then chosen, such as a maximum in the stress-strain curve, and a constitutive equation is assumed. By inserting the

instability criterion and the constitutive equation in the equation of state, a critical strain for the initiation of FLITE can then be derived. A good example of such an analysis can be found in the paper by Culver [9]. From this and other analyses of this type, it has become clear that for a high resistance to FLITE, materials should rapidly strain harden, have a low strength and a high resistance to thermal softening.
In recent years, it has become clear that the prediction of a critical strain is not enough to adequately describe FLITE. This is because in reality FLITE is a time-dependent process, and not an instantaneous event. Therefore, Semiatin and co-workers [26, 34, 55] proposed a so-called Flow Localization Parameter (FLP) to describe FLITE. This FLP is defined as follows:

$$FLP = \frac{1}{\dot{\varepsilon}} * \frac{\delta \dot{\varepsilon}}{\delta \varepsilon} \qquad (1)$$

It can be obtained by assuming that a deforming material can be separated into two regions: one containing an initial geometric, material or deformation process defect or temperature gradients [11], the other homogeneous. By enforcing equilibrium of the load supported by the two regions, the FLP can be derived. The FLP can be expressed in terms of critical strain and current strain; if the current strain is equal to the critical strain the FLP has a value of zero. According to Semiatin et al., noticeable flow localization occurs when the FLP has reached a value of approximately five.
This approach to FLITE as a time-dependent process is important for describing flow after the instability strain has been attained. The exact use of this approach to FLITE in production technology remains at this moment unclear, but it may well be that it enables further refinement and optimization of the FLITE criteria currently employed.

3. A GENERAL THEORY OF FLITE

3.1 Introduction

In this chapter, a general theory of FLITE will be developed by deriving a load, local and thermal instability criterion. Semiatin et al.'s approach to instability problems will also be included.

3.2. Assumptions

The following assumptions are made:
- there is an equation of state of the form $\sigma = \sigma(\varepsilon, \dot{\varepsilon}, T)$, with σ the effective stress, ε the effective strain, $\dot{\varepsilon}$ the effective strain rate and T the temperature.
- there is a plane stress situation and a straight stress path.
- the constitutive equation has the form $\sigma = K * \varepsilon^n * \dot{\varepsilon}^m * h(T)$, with K a material constant, n the strain hardening exponent, m the strain rate hardening exponent and h(T) an unspecified function of the temperature.

All equations will be presented in terms of effective stress σ and effective strain ε or in terms of principal stresses σ_1, σ_2 and σ_3 and principal strains ε_1, ε_2 and ε_3.

3.3. Load instability criterion

Assume a volume element with dimensions x_1, x_2 and x_3 (fig. 1). The principal stresses are given by:

$$\sigma_2 = i * \sigma_1, \quad \sigma_3 = 0 \qquad (2)$$

where i is the stress path.
If we number the principal stresses in such a way that F_1 ($= \sigma_1 * A_1$, with A_1 the surface of the volume element in the 1-direction) is the largest force, load instability will occur when $dF_1 = 0$, or:

$$\sigma_1 * dA_1 + d\sigma_1 * A_1 = 0 \qquad (3)$$

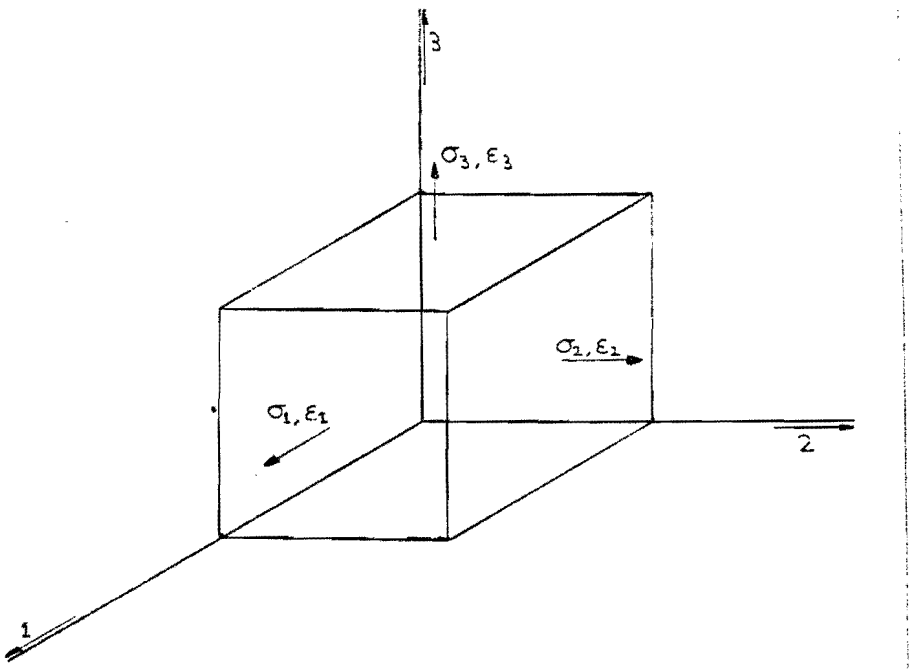

Fig. 1. The volume element x_1, x_2, x_3 with principal strains and stresses.

From (3), the following critical strain for the initiation of FLITE by load instability can be derived (for the necessary calculations see appendix A):

$$\varepsilon_c = \frac{n}{-\frac{m}{\varepsilon} * \frac{d\dot{\varepsilon}}{d\varepsilon} - \frac{\partial\sigma}{\partial T} * \frac{\alpha}{\varrho * c} + \frac{2 - i}{2 * I}} \qquad (4)$$

where ε_c is the critical strain, $\frac{\partial\sigma}{\partial T}$ the temperature dependence of stress, α the fraction of heat retained within the material ($\alpha = 1$ is adiabatic), ϱ the specific weight, c the specific heat and $I = \sqrt{(i^2 - i + 1)}$.
Since the effective strain rate can be assumed to be constant before localization occurs, the strain rate term can be neglected, and we finally obtain:

$$\varepsilon_c = \frac{n}{-\frac{\partial\sigma}{\partial T} * \frac{\alpha}{\varrho * c} + \frac{2 - i}{2 * I}} \qquad (5)$$

3.4. Local instability criterion

To obtain a criterion for FLITE by local instability, we need an expression for plastic work done per unit volume:

$$dW_s = \sigma * d\varepsilon \qquad (6)$$

where dW_s is plastic work per unit volume.
Kals [1] states that instability will occur when the dissipation of work per unit surface increase shows a maximum, or:

$$\frac{d}{dA_3}\left(\frac{dW_s}{dA_3}\right) = 0 \qquad (7)$$

where dA_3 is a surface element normal to the third principal direction.
The following critical strain can be derived from (7) (see appendix A for the necessary calculations):

$$\varepsilon_c = \frac{2 * I}{1 + i} * \frac{n}{(m + 1) - \frac{\alpha}{\varrho * c} * \frac{\partial \sigma}{\partial T} * \frac{2 * I}{1 + i}} \qquad (8)$$

3.5. Thermal instability criterion

FLITE by thermal instability is said to initiate when the flow stress passes through a maximum, or:

$$d\sigma = 0 \qquad (9)$$

Equation (9) leads to the following critical strain (see appendix A for the necessary calculations):

$$\varepsilon_c = \frac{n}{-\frac{m}{\dot{\varepsilon}} * \frac{d\dot{\varepsilon}}{d\varepsilon} - \frac{\partial \sigma}{\partial T} * \frac{\alpha}{\varrho * c}} \qquad (10)$$

Once again, the strain rate is constant until localization initiates, so we can neglect the strain rate term to obtain:

$$\varepsilon_c = -\frac{\varrho * c * n}{\alpha * \frac{\partial \sigma}{\partial T}} \qquad (11)$$

3.6. Flow Localization Parameter (FLP)

We will now assume that the volume element x_1, x_2, x_3 consists of two regions: one containing an initial defect as discussed in 2.2., the other homogeneous. The FLP can be obtained from a variational analysis carried out to determine the conditions under which the load supported by the two regions remains equal. Once again, we consider the first principal direction to be the critical direction. The variational equilibrium condition can then be expressed as follows:

$$\delta F_1 = \delta(\sigma_1 * A_1) = \sigma_1 * \delta A_1 + \delta\sigma_1 * A_1 = 0 \qquad (12)$$

From equation (12) three FLP's can be derived: a load, local and thermal instability FLP (for the necessary calculations see appendix B). Only the load instability FLP, however, is physically possible, since from the other two it follows that flow localizes before instability has initiated. Therefore only the load instability FLP is presented here. This FLP can be expressed as follows:

$$FLP = (\frac{n}{\varepsilon_c} - \frac{n}{\varepsilon})/m \qquad (13)$$

Equation (13) completes the general theory of FLITE.

3.7. The general theory of FLITE compared to the literature

In this paragraph, the results from paragraphs 3.3., 3.4., 3.5. and 3.6. will be compared with the literature.

- Load instability criterion.
  The critical strain obtained from the load instability analysis was:

$$\varepsilon_c = \frac{n}{-\frac{\partial\sigma}{\partial T} * \frac{\alpha}{\varrho * c} + \frac{2 - i}{2 * I}} \qquad (5)$$

  If we compare (4) with the result obtained by Kals [1], which is:

$$\varepsilon_c = \frac{2 * I}{2 - i} * n \qquad (13)$$

and was obtained without considering strain rate or thermal effects, we see that his result can be obtained from (5) by neglecting thermal effects.

- Local instability criterion

The result obtained from the local instability analysis was:

$$\varepsilon_c = \frac{2 * I}{1 + i} * \frac{n}{(m + 1) - \frac{\alpha}{\varrho * c} * \frac{\partial \sigma}{\partial T} * \frac{2 * I}{1 + i}} \qquad (8)$$

Kals' [1] result was:

$$\varepsilon_c = \frac{2 * I}{1 + i} * n \qquad (14)$$

Once again, this result, which was obtained without considering strain rate or thermal effects, can be derived from (8) by neglecting thermal effects.

- Thermal instability analysis

The result obtained from the thermal instability analysis was:

$$\varepsilon_c = - \frac{\varrho * c * n}{\alpha * \frac{\partial \sigma}{\partial T}} \qquad (11)$$

This result is identical to the results obtained by Culver [9], Dautzenberg [1], Semiatin et al. [26], and others.

- The Flow Localization Parameter

The FLP derived in 3.6. is identical to the one derived in [26] by Semiatin et al. Semiatin et al.'s FLP, however, is based on a thermal instability criterion in torsion, and not on a load instability criterion for all stress paths.

This concludes our comparison of the FLITE theory derived in this chapter with the literature.

3.8. Discussion of the general theory of FLITE

There are two things about the general theory of FLITE that should be discussed further: the influence of the strain rate on the instability criteria and the FLP obtained in 3.6.
In the load and thermal instability criteria, an increasing value of the strain rate hardening exponent m means a higher critical strain (see (4) and (10)), but in the local instability criterion a higher m-value means a lower critical strain. This is probably the result of two contradictory mechanisms: for a high resistance to FLITE, materials should rapidly strain harden, and since the effect of strain rate hardening is qualitatively the same, it logically follows that they should also exhibit rapid strain rate hardening. This is expressed in the load and thermal instability criteria. It is also true, however, that for a high resistance to FLITE materials should have a low strength. Since there is a critical flow stress accompanying the critical strain, it follows from the constitutive equation assumed that this stress will be reached sooner for a higher m-value, which is what is expressed in the local instability strain. That this effect is not included in the load and thermal instability criteria is probably due to the fact that these are derived by a purely mechanical analysis based on the equation of state assumed, whereas the local instability criterion is derived by carrying out an energy analysis of the deformation process.
The FLP derived in 3.6. has the same form as the one derived by Semiatin et al., but it is based on a load instability analysis and not on a thermal instability analysis. The difference between the two is that the load instability FLP is also valid for isothermal deformation, since the load instability strain is defined for isothermal as well as non-isothermal deformation processes, whereas the thermal instability FLP is only valid for non-isothermal deformation processes. Because of this, the load instability criterion seems preferable. This unfortunately implies that the value of the FLP for the onset of noticeable localization set by Semiatin et al. can no longer be used. This value will therefore have to be determined again for the load instability FLP.

4. EXPERIMENTS

4.1. Introduction

To test the general theory of FLITF developed in the previous chapter, the following experiments were carried out:

- high-speed tensile tests on Al51St (an aluminum alloy), polyvinylchloride (PVC) and polycarbonate (PC).
- application of the general theory to experimental data from the literature.

4.2. The high speed tensile tests

For the high speed tensile tests a **Zwick r_{el} type 1852** hydraulic tensile testing machine was used. Tensile test bars were made according to DIN 50125 (Al51St) and DIN 53455 (PVC, PC) specifications. In table 1, the relevant material properties are given. These were obtained from **[4]** and **[54]**, with the exception of the values of $\frac{\partial \sigma}{\partial T}$ for PVC and PC, which I obtained myself. Due to the limitations of the experimental method used (see appendix C), these should be interpreted as rough estimates of the actual values. Because of its very small influence, the strain rate hardening exponent has been omitted (in the load and thermal instability criteria it is absent because the strain rate is constant until instability occurs, and in the local instability criterion its influence is approximately 2%). The results of the experiments can be found in table 2. In appendix C, more detailed information is given.
The rest of this paragraph will be used to discuss the results from table 2.

- the value of α was taken from **[2]** for Al51St. Because of the expected adiabaticity of the tensile tests on PVC and PC, α was set at 1 for these materials.
- ε_{cload}, ε_{cloc} and ε_{cth} were calculated from **(5)**, **(8)** and **(11)**, with $i = 0$.
- ε_{cexp} was obtained from the maximum in the stress strain curves.
- ε_f was obtained by measuring the width and thickness of the test specimen as close to the fracture as possible.

- all tests were carried out at room temperature.

Material	ϱ [kg*mm^{-3}]	c [mJ*kg^{-1}*K^{-1}]	$\frac{\partial \sigma}{\partial T}$ [N*mm^{-2}*K^{-1}]	n [-]
Al51St	2.7 E-06	9.6 E 05	-.3	.06
PVC	1.4 E-09	1.2 E 06	-.7	.05
PC	1.2 E-09	1.2 E 06	-.3	.03

Table 1. Material properties.

Material	α [-]	ε_{cload} [-]	ε_{cloc} [-]	ε_{cth} [-]	ε_{cexp} [-]	ε_{f} [-]	$\dot{\varepsilon}$ [s^{-1}]
Al51St	.7	.06	.11	.85	.19	.20	10
PVC	1	.0001	.0001	.0001	.07	.40	100
PC	1	.0001	.0001	.0001	.12	---	75

Table 2. Experimental results. Subscripts cload, cloc, cth, cexp and f denote predicted load, local and thermal instability strains, experimental instability strain and fracture strain, respectively.

Al51St

Al51St unexpectedly fractured immediately after experimental instability, without noticeable signs of FLITE, such as shear bands (narrow bands of extremely localized deformation, often colored differently)(fig. 1). It turned out that it had been heat-treated to obtain a higher strength, which explains the low value of the fracture strain.

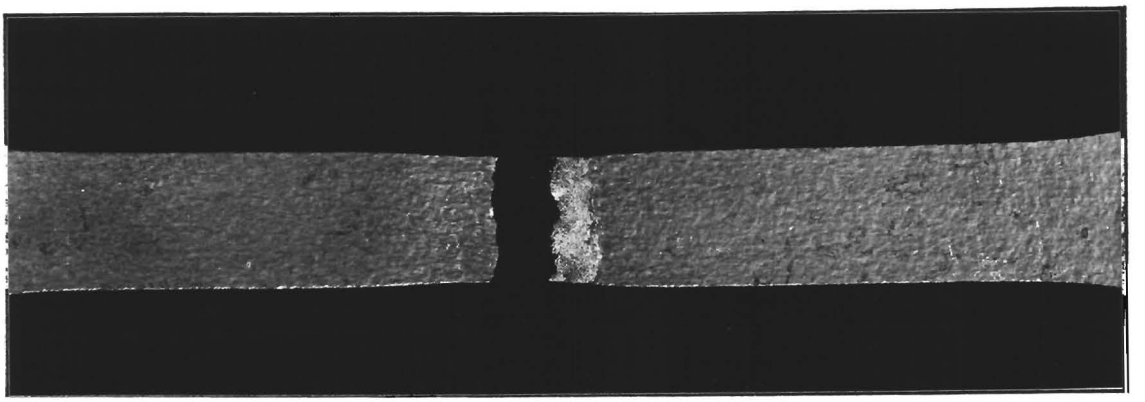

Fig. 1. A fractured Al51St specimen.

PVC

PVC fractured at a strain of more than five times its experimental instability strain. Immediately after fracture, the region around the fracture expanded visibly and regained its original dark red color (fig. 2, upper specimen). The remainder of the specimen had turned white, which is a sign of localized deformation. For a comparison, isothermal tests on PVC were carried out. In this case, the region around the fracture did not expand. Localized deformation did occur, but did not spread evenly over the entire specimen (fig. 2, lower specimen).

It is likely that the expanding of the region around the fractured was caused by the elastic recovery of the material after fracture. This effect is well known in injection molding, where it is called 'die swell'. It is caused by the following mechanism: during the tensile test, the molecules of the plastic orient themselves in the direction of the tensile force. After fracture, they recover their original globular orientation, accompagnied by swelling up to their original volume.

That this effect is at least partly thermally influenced is shown in fig. 3: the fracture region from the lower specimen from fig. 2 was immersed in boiling water for approximately ten seconds, causing it to swell up to its original dimensions and regain its red color. This is obviously a thermal effect, which leads to the conclusion that the die swell exhibited by the upper specimen in fig. 2 is also caused (at least partly) by thermal effects. This thermal effect is caused by the near adiabaticity of the high-speed tensile tests.

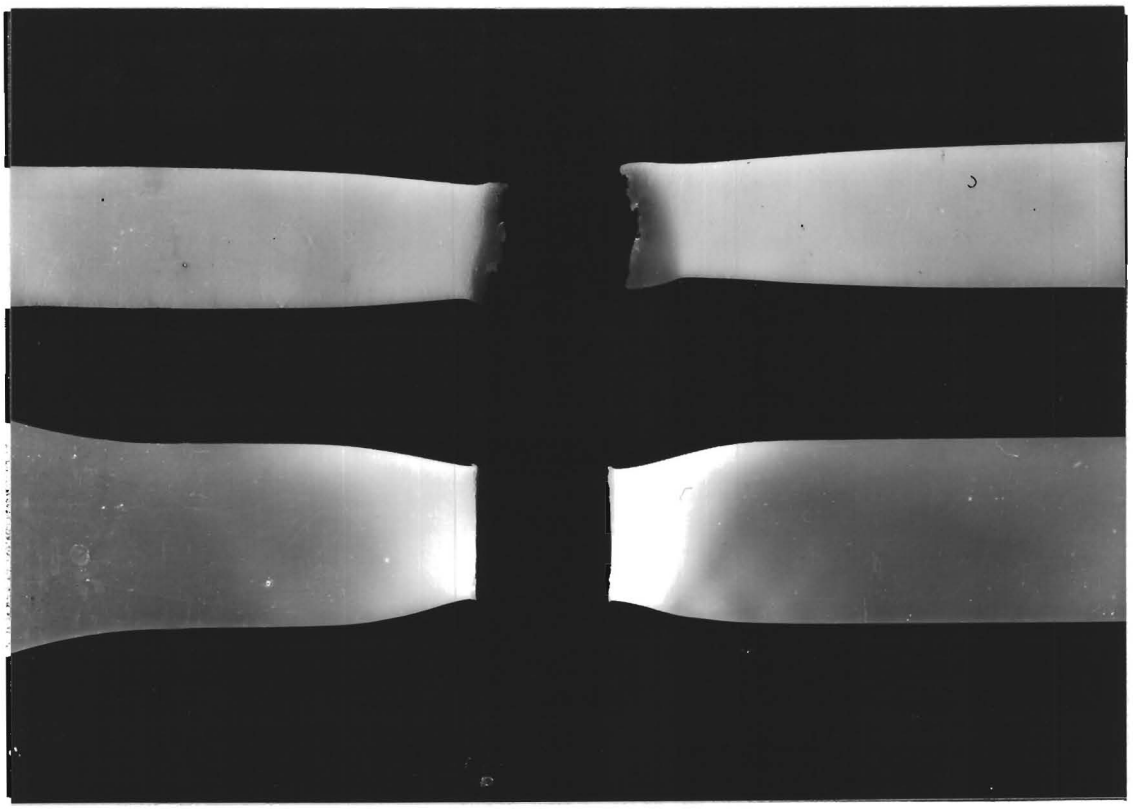

Fig. 2. Fractured PVC specimens: upper specimen tested at a very high strain rate, lower specimen tested at a low strain rate.

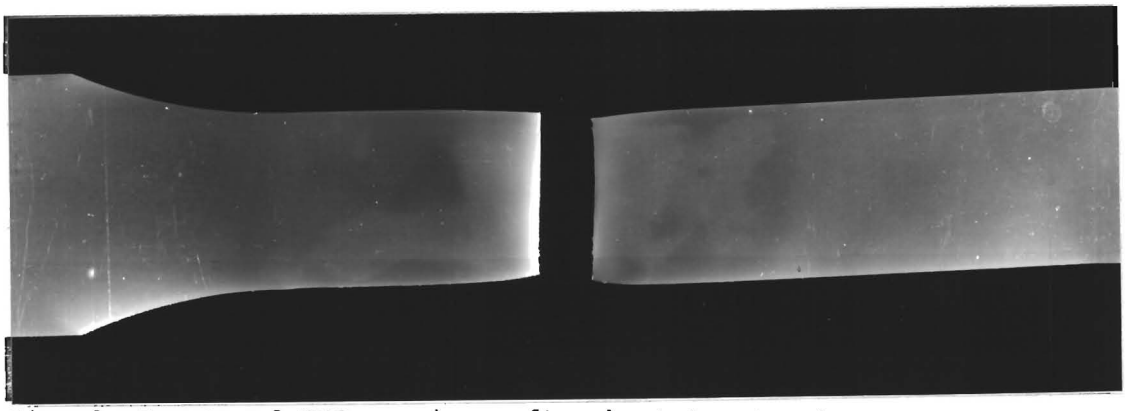

Fig. 3. Fractured PVC specimen after heat treatment.

PC

The PC results are similar to those of PVC, but, due to the insufficient stroke of the tensile testing machine, the PC specimens did not fracture. After instability, the deformation continued homogeneously, like it did in PVC. This is illustrated in fig. 4, in which the upper specimen is untested.

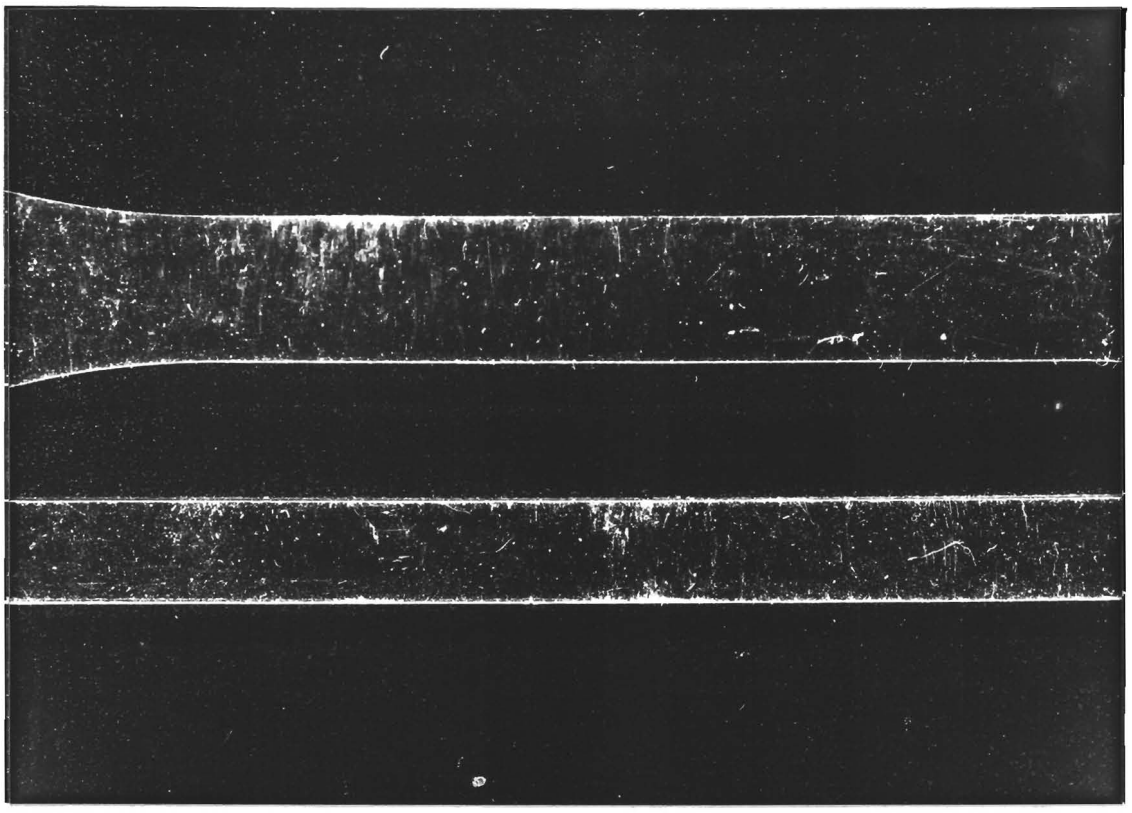

Fig. 4. PC specimens: upper specimen untested, lower specimen tested at a high strain rate.

The experimental and theoretical instability strains

Unfortunately, it must be concluded that the predicted instability strains only partly cover the results of Al51St and do not cover the results of the plastics at all. It was expected that the actual instability strains would lie somewhere between the local and thermal instability strains predicted, with fracture occurring after the thermal instability strain. For Al51ST, fracture occurred too soon, which, as has been said, may be attributed to the heat treatment the specimens had undergone. The predicted instability strains for the plastics are totally unrealistic: all three lie in the elastic range of the material.

Therefore it must be concluded that the general theory of FLITE is not valid for PVC and PC, which is probably due to the assumption of a power-law type of constitutive equation. Although there is evidence [50] that there are conditions under which such a constitutive equation is valid for plastics, this is by no means generally true. Further investigations in this direction, therefore, seem desirable.

4.3. The general theory of FLITE applied to data from the literature

To further evaluate the general theory of FLITE, it was applied to data from [3] and [9]. In both cases, impact torsion tests were performed on a number of materials. For the results, see table 3.

Material	ε_{cload} [-]	ε_{cth} [-]	ε_{cexp} [-]	ε_{f} [-]
Al 6061-T6	.06	.59	.17	.74
Al51St	.04	.66	.13	1.2
Ti	.12	.53	.51	.64
Ti 6Al-4V	.05	.16	.17	.60

Table 3. Experimental results from the literature.

The experimental data for Al 6061-T6 and Ti were obtained from [9], the others from [3]. The load and thermal instability strains were calculated from (5) and (8), with α set at .9 and i at -1.
In this case, the FLITE theory worked well: the actual instability strain was reached before or just at the thermal instability strain, which is theoretically the upper limit for instability. Fracture occurred after the thermal instability strain had been passed, with Al51ST exhibiting a fairly high fracture strain.

4.4. The FLP applied to the experimental data

In accordance with Semiatin et al.'s method, FLP's were calculated at the fracture strain. The strain rate hardening exponents were obtained from [55]. No strain rate hardening exponent was obtained for Al51St, and FLP's for PVC and PC were not calculated. The results are presented in table 4.

[55]. No strain rate hardening exponent was obtained for Al51St, and FLP's for PVC and PC were not calculated. The results are presented in table 4.

Material	m [-]	ε_f [-]	FLP_{load} [-]	FLP_{th} [-]
Al 6061-T6	.002	.74	766	17
Ti	.025	.64	46	2.2
Ti 6Al-4V	.015	.60	86	21

Table 4. The Flow Localization Parameters.

The load instability FLP was calculated from (13). The thermal instability FLP was also calculated from (13), but with the thermal instability strain inserted.
The agreement between Semiatin et al.'s FLP and these results is good. Culver [9] found no noticeable localization in Ti, which corresponds to an FLP of less than five. He did find extreme localization in Al 6061-T6, which is what is expected from the value of the FLP. Whether noticeable localization occurred in Ti 6Al-4V is not known, since this was not investigated by Sillekens [3].
Not much can be said about the load instability FLP's accuracy in predicting the occurrence of noticeable localization since we do not have a minimum value of this FLP for noticeable localization. Finding such a minimum value will require much additional research.

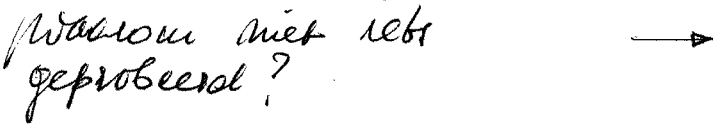

5. CONCLUSIONS

5.1. Discussion of the FLITE theory and the experimental results

In this report, a theory has been derived to describe thermally influenced flow localization phenomena during manufacturing processes at room temperature. Three criteria were used to obtain the strain at which flow theoretically starts to localize: a maximum in load, a maximum in the dissipation of work per unit surface increase and a maximum in flow stress. The strains associated with these criteria are called load, local and thermal instability strains, respectively. Since these strains by themselves do not sufficiently describe the process of flow localization (labeled FLITE in this report), a so-called Flow Localization Parameter (FLP) was derived to describe flow after localization has begun. This FLP and the three instability strains comprise the general theory of FLITE, which has been tested on metals and plastics. From the results, we can draw the following conclusions:

- the theory cannot predict accurate instability strains for PVC and PC. This is probably caused by the power-law type constitutive equation assumed. A different constitutive equation might solve this problem.
- the actual instability strains for metals lie somewhere between the predicted load and thermal instability strains. In the tensile test, the actual instability strain lies between the local and thermal instability strains. Fracture occurs after the thermal instability strain has been passed.
- the FLP is a good instrument to describe flow after instability. It is probably best to use an FLP based on the load instability criterion, since it is then defined for isothermal as well as non-isothermal deformation processes. A minimum value for this FLP at the onset of noticeable flow localization will have to be derived.

In general, the first indications are that the theory of FLITE derived in this report will have useful engineering applications. These will be described in the following paragraph.

5.2 Application of the general theory of FLITE

For isothermal or near isothermal conditions, the instability criteria derived by Kals [1] can be used. These may be derived from the general theory of FLITE by neglecting thermal effects, so that a load and local instability criterion are obtained (there is no thermal instability criterion for isothermal deformation). Kals showed that the load instability criterion determines the initiation of flow localization for positive first and second principal strains and the local instability criterion determines the initiation of flow localization for positive first and negative second principal strains. This may be shown graphically in a so-called forming limit diagram, which gives the loci of the first and second principal strains at instability (fig. 5).

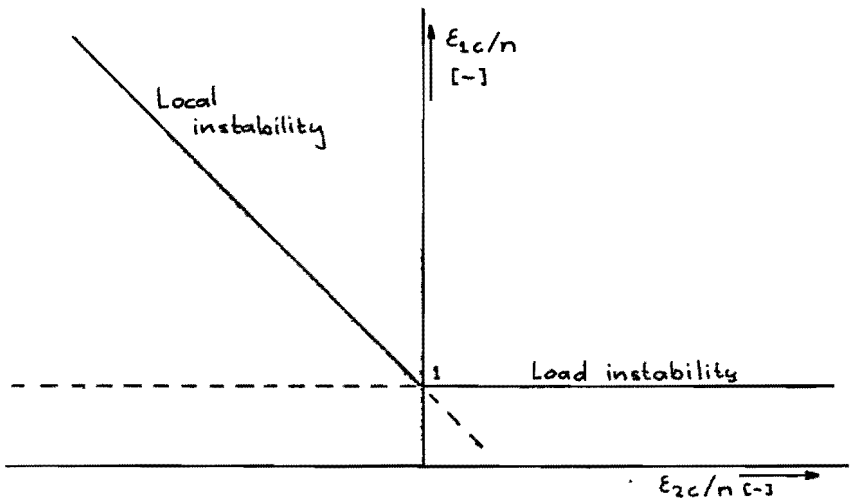

Fig. 5. The forming limit diagram.

For non-isothermal conditions, i.e. manufacturing processes with effective strain rates greater than five, the complete FLITE theory must be used to determine the instability strains. Unfortunately, the results are difficult to represent graphically, since the forming limit diagrams are dependent on the stress path in the non-isothermal case. Instead, a diagram representing the effective instability strains as a function of the stress path can be drawn. These are dependent on the thermophysical properties of the materials represented, but in general look like fig. 6.

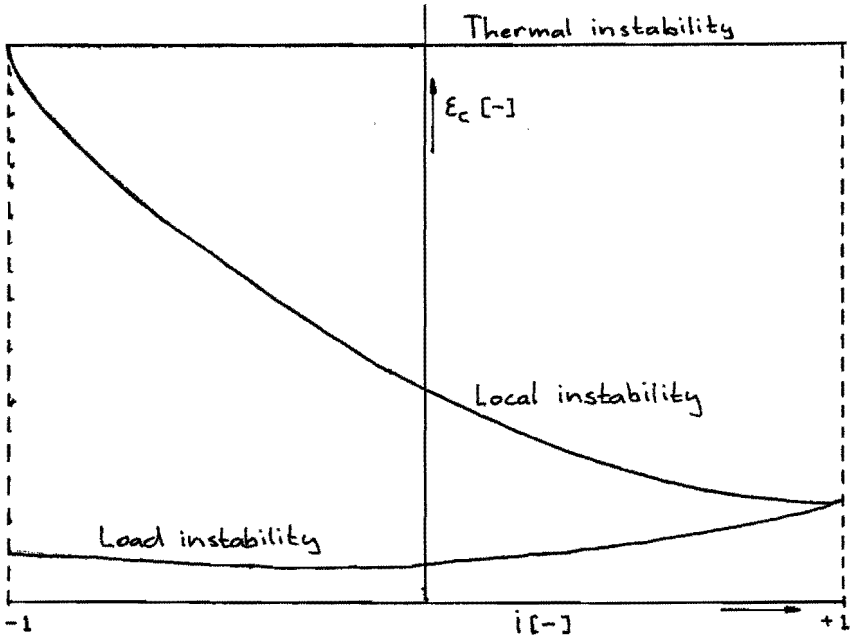

inclusief thermische invloeden.

Fig. 6. Effective instability strain as a function of stress path.

The following approach to using the FLITE theory as a designing tool can now be taken:

Step 1. The stress path is determined and the critical instability strains are calculated.

Step 2. The effects of flow localization are analysed. The result of this analysis should be: no flow localization permissible, limited flow localization permissible or flow localization unimportant, in which case fracture is the determining factor.

Step 3. For the three cases described above, there are three values of the FLP (which is still based on load instability). These values (which are not yet known and require further research) correspond to specific maximum strains. These are now calculated.

Step 4. The strains calculated in step 3 are used to design the product and its production process.

In this way, the FLITE theory may be used as a designing tool. Some of its possible applications are in bending [1], deep-drawing [1], extrusion (to determine the occurrence of a dead zone), blanking (to obtain the process parameters which result in smooth-sheared products) and metalcutting (to

obtain the critical cutting speed for minimal surface roughness). Many other manufacturing processes probably exhibit FLITE or FLITE-related phenomena. The challenge for the future will be to identify those processes hampered by FLITE and with the help of adequate process descriptions, finding a solution for these problems.

6. FINAL REMARKS

I would like to end this report with a few reflections on the methods I used to carry out my graduation research project.
When I started working on this project, my thinking on the methodology of scienticic research had already been strongly influenced by the works of Karl Popper. In Popper's view, one should not try to obtain scientific theories by inductivist methods. Instead, a theory describing the phenomena one is interested in should be derived before carrying out experiments. Experiments should then be carried out to test the theory. Should the experimental results contradict the theory, the theory is falsified and a new theory must be derived. This process is repeated until an adequate theory is obtained.
While reading papers on FLITE for the literature survey, I discovered that most of them are of an inductivist nature. While it is always possible that plausible results are obtained this way, I prefer Popper's approach myself. So, after having completed the literature survey, I spent the next few months trying to obtain one general theory covering all FLITE phenomena. Of course, I did not succeed. There is probably no single theory covering all FLITE phenomena, but even if there were one, it is highly unlikely that a graduate student with no previous experience in FLITE research would find it. After having somewhat belatedly realized this, I concentrated my efforts on FLITE in plastic deformation at room temperature. By combining the results of several earlier authors and adding some theoretical work of myself, I was able to derive a theory describing these phenomena. The next problem was how to test this theory. The established way would have been to carry out impact torsion tests, but since doing this would have added nothing new to FLITE research, I opted for the high-speed tensile test instead. Fortunately, EUT's Department of Chemical Technology owned a high-speed tensile testing machine. Unfortunately, due to the budget cuts that have been imposed on EUT (and all other Dutch universities and colleges), the number of experiments I could carry out was limited. Therefore, I could not, in good faith, draw anything more than preliminary conclusions from my experimental results. Much more testing will be necessary before any definitive conclusions about the validity and usefulness of my theory are

possible. I do hope, however, that even should my theory have to be rejected, the way of thinking behind my theory will be used long after my theory has been forgotten, and that in this way I will have contributed something to FLITE research.

REFERENCES

1. Omvormtechnologie A, reader nr. 4.558
   J.A.G. Kals et al., Eindhoven University of Technology, 1983
2. Numerieke methode voor de bepaling van de temperatuursverdeling in een torsiestaaf tijdens plastische deformatie
   M.P. Snijder van Wissenkerke, WPB-report nr. 0091, EUT, 1981
3. Thermische instabiliteit bij torsie
   W.H. Sillekens, WPA-report nr. 0347, EUT, 1986
4. Het torsiemoment bij thermische instabiliteit
   J.H. van Liempd, WPA-report nr. 0377, EUT, 1987
5. Catastrophic thermoplastic shear
   R.F. Recht, J. Applied Mechanics, vol. 31, 189, 1964
6. On a class of thermomechanical processes during rapid plastic deformation
   B.F. von Turkovich, Annals of the CIRP, vol. 21, 15, 1972
7. Large strain, high strain rate testing of copper
   U.S. Lindholm et al., J. Eng. Mat. Techn., Trans. ASME, vol. 102, 376, 1980
8. Effect of strain rate upon plastic flow
   C. Zener et al., J. Applied Physics, vol. 15, 22, 1944
9. Thermal instability strain in dynamic plastic deformation
   R.S. Culver, Metallurgical effects at high strain rates, 519, Plenum Press, 1973
10. The relation between adiabatic shear instability strain and material properties
    M.R. Staker, Acta Metall., vol. 29, 683, 1981
11. An analysis of flow localization during torsion testing
    E. Rauch et al., Acta Metall., vol. 33, 465, 1985
12. Effect of deformation heating and strain rate sensitivity on flow localization during the torsion testing of 6061 aluminum
    S.L. Semiatin et al., Acta Metall., vol. 34, 167, 1986
13. Tensile and shear instabilities in tensile tests on rods and sheets
    Y. Bai et al., Metals Techn., vol. 8, 420, 1981
14. Plugging: physical understanding and energy absorption

Y. Bai et al., Metals Techn., vol. 9, 182, 1982

15. Modeling of adiabatic shear band development from small imperfections
A.M. Merzer, J. Mech. Phys. Solids, vol. 30, 323, 1982

16. Shear instabilities in blanking and related processes
B. Dodd, Metals Techn., vol. 10, 57, 1983

17. The structure of adiabatic shear bands in metals: a critical review
S.P. Timothy, Acta Metall., vol. 35, 301, 1987

18. Adiabatic instability in the orthogonal cutting of steel
J.C. Lemaire et al., Met. Trans., vol. 3, 477, 1972

19. Adiabatic shearing - general nature and material aspects
H.C. Rogers, Material behavior under high stress and ultra-high strain rates, 101, Plenum Press, 1983

20. Stress-strain curves of some metals and alloys at low temperatures and high rates of strain
H.G. Baron, J. Iron and Steel Inst., vol. 182, 354, 1956

21. The propagation of adiabatic shear
M.E. Backman et al., Metallurgical effects at high strain rates, 531, Plenum Press, 1973

22. Adiabatic platic deformation
H.C. Rogers, Ann. Rev. Mater. Sci., 283, 1979

23. A thermo-plastic shear instability criterion applied to surface cracking in upsetting and related processes
A. Jenner et al., J. Strain Analysis, vol. 16, 159, 1981

24. Thermo-plastic instability in simple shear
Y. Bai, J. Mech. Phys. of Solids, vol. 30, 195, 1982

25. Metallurgical effects on impact loaded materials
K. Hartmann et al., Shock waves and high strain rate phenomena in metals, 325, Plenum Press, 1981

26. Plastic instability and flow localization in shear at high rates of deformation
S.L. Semiatin et al., Acta Metall., vol. 32, 1347, 1984

27. Deformation reelle au cours du filage
J. Buffet et al., Revue de Metallurgie, vol. 57, 827, 1960

28. Ductile fracture of aluminum
G.Y. Chin et al., Trans. AIME, vol. 230, 437, 1964

29. Influence of the mechanical loading system on low-temperature plastic instability
G.Y. Chin et al., Trans. AIME, vol. 230, 1043, 1964
30. Apercu sur la plasticite adiabatique
J. Pomey, Annals of the CIRP, vol. 23, 93, 1966
31. The phenomenon of adiabatic shear deformation
A. Bedford et al., J. Aust. Inst. Metals, vol. 19, 61, 1974
32. An explanation of adiabatic shear
R. Bish, J. Aust. Inst. Metals, vol. 21, 114, 1976
33. Shear strains, strain rates and temperature changes in adiabatic shear bands
G.L. Moss, US Army report ARBRL-TR-02242
34. The occurence of shear bands in metalworking
S.L. Semiatin et al., Material behavior under high stress and ultra-high loading rates, 129, Plenum Press, 1983
35. Microstructural damage adjacent to bullet holes in 70-30 brass
J.V. Craig et al., J. Aust. Inst. Metals, vol. 15, 1, 1970
36. Reversal of Fe-Ni-C martensite by rapid large shear
R.J. Russell et al., Met. Trans., vol. 3, 2403, 1972
37. Investigations into the prevention of adiabatic shear failure in high strength armour materials
J.M. Yellup et al., Res Mechanica, vol. 1, 41, 1980
38. Adiabatic deformation and strain localization
G.B Olson et al., Shock waves and high strain rate phenomena in metals, 221, Plenum Press, 1981
39. Metallurgical influences on shear band activity
D.A. Shockey et al., ibid., 249
40. A criterion for thermo-plastic shear instability
Y. Bai, ibid., 277
41. Materials factors in adiabatic shearing in steels
H.C. Rogers et al., ibid., 285
42. A criterion for inhomogeneous plastic deformation
P.B. Bowden, Phil. Mag., vol. 22, 455, 1970
43. The formation of micro shear bands in PS and PMMA
P.B. Bowden et al., ibid., 463

44. Adiabatic shear of titanium and PMMA
R.E. Winter, Phil. Mag., vol. 31, 765, 1975
45. The initiation and growth of adiabatic shear bands
T.W. Wright et al., Int. J. Plasticity, vol. 1, 1985
46. Technische plasticiteitsleer, reader nr. 4406
P.C. Veenstra et al., Eindhoven University of Technology, 1984
47. Strain, stresses and forces in blanking
J.A.H. Ramaekers et al., Research in manufacturing technology, University of Galway, 1986
48. The relation between effective deformation and micro-hardness in a state of large plastic deformation
J.A.H. Ramaekers et al., Annals of the CIRP, vol. 28, 541, 1970
49. De Nadaise verstevigingsfunctie van PE, bepaald m.b.v. een geautomatiseerde trekproef
A.H.A.M. Vriens, IHBO Tilburg, 1972
50. J.A.H. Ramaekers, private communication
51. Theory of the tensile test
E.W. Hart, Acta Metall., vol. 15, 351, 1967
52. Strain rate dependent plastic flow behavior of metals
D. Lee et al., The inhomogeneity of plastic deformation, 113, ASM, 1973
53. Stability of plastic deformation
A.S. Argon, ibid., 161
54. L. Govaert, private communication
55. Formability and workability of metals - plastic instability and flow localization
S.L. Semiatin and J.J. Jonas, ASM, 1984

Appendix A. Calculation of the critical instability strains.

A.1. Load instability.

The principal stresses are given by:

$$\sigma_2 = i * \sigma_1 \; ; \; \sigma_3 = 0 \qquad (a.1.)$$

With (a.1.), the stress - strain relationships according to Lévy-von Mises can be expressed as follows:

$$d\varepsilon_1 = \frac{d\lambda}{2} * \sigma_1 * (2 - i) \qquad (a.2.)$$

$$d\varepsilon_2 = \frac{d\lambda}{2} * \sigma_1 * (2 * i - 1) \qquad (a.3.)$$

$$d\varepsilon_3 = \frac{d\lambda}{2} * \sigma_1 * (1 + i) \qquad (a.4.)$$

This leads to the following expression for the effective strain increment $d\bar{\varepsilon}$:

$$d\bar{\varepsilon} = \frac{2 * I}{2 - i} * d\varepsilon_1 = \frac{2 * I}{2*i - 1} * d\varepsilon_2 = \frac{-2 * I}{1 + i} * d\varepsilon_3 \qquad (a.5.)$$

with $I = \sqrt{(i^2 - i + 1)}$.
Since i is assumed to be constant, (a.5.) can be easily integrated, which results in:

$$\bar{\varepsilon} = \frac{2 * I}{2 - i} * \varepsilon_1 = \frac{2 * I}{2*i - 1} * \varepsilon_2 = \frac{-2 * I}{1 + i} * \varepsilon_3 \qquad (a.6.)$$

Load instability occurs when $dF_1 = 0$ (see 3.3.), or:

Zie ongenummerde
mogelijkheid op blad
Anarch. p. 12 →

$$\sigma_1 * dA_1 + d\sigma_1 * A_1 = 0 \qquad (a.7.)$$

With $\frac{dA_1}{A_1} = -d\varepsilon_1$, (a.7.) can be rewritten as:

$$\sigma_1 = \frac{d\sigma_1}{d\varepsilon_1} \qquad (a.8.)$$

Using (a.5.) and the relations $\bar{\sigma} = I * \sigma_1$, $d\bar{\sigma} = I * d\sigma_1$, (a.8.) can be rewritten as:

$$\frac{2 * I}{2 - i} * \frac{d\bar{\sigma}}{d\bar{\varepsilon}} - \bar{\sigma} = 0 \qquad (a.9.)$$

With the assumption of $\bar{\sigma} = \bar{\sigma}(\bar{\varepsilon}, \dot{\bar{\varepsilon}}, T)$, we can write $\frac{d\bar{\sigma}}{d\bar{\varepsilon}}$ as follows:

$$\frac{d\bar{\sigma}}{d\bar{\varepsilon}} = \left(\frac{n}{\bar{\varepsilon}} + \frac{m}{\dot{\bar{\varepsilon}}} * \frac{d\dot{\bar{\varepsilon}}}{d\bar{\varepsilon}}\right) * \bar{\sigma} + \frac{\partial\bar{\sigma}}{\partial T} * \frac{dT}{d\bar{\varepsilon}} \qquad (a.10.)$$

For dT, we have the following expression:

$$dT = \frac{\alpha * \bar{\sigma} * d\bar{\varepsilon}}{\rho * c} \qquad (a.11.)$$

With (a.10.) and (a.11), we can write (a.9.) as:

$$\frac{2 * I}{2 - i} * \left(\frac{n}{\bar{\varepsilon}} + \frac{m}{\dot{\bar{\varepsilon}}} * \frac{d\dot{\bar{\varepsilon}}}{d\bar{\varepsilon}} + \frac{\partial\bar{\sigma}}{\partial T} * \frac{\alpha}{\rho * c} - \frac{(2 - i)}{2 * I}\right) * \bar{\sigma} = 0 \qquad (a.12.)$$

Instability will occur when the expression in parentheses first becomes zero. This leads to the following critical strain:

$$\bar{\varepsilon}_c = \frac{n}{-\frac{m}{\dot{\bar{\varepsilon}}} * \frac{d\dot{\bar{\varepsilon}}}{d\bar{\varepsilon}} - \frac{\partial \bar{\sigma}}{\partial T} * \frac{\alpha}{\rho * c} + \frac{2-i}{2 * I}} \qquad (a.13.)$$

This is the critical strain for FLITE by load instability.

A.2. Local instability.

We start this analysis the same way as the previous one, with eqs. (a.1.) through (a.6.). To arrive at an instability criterion, we consider a surface element A_3. With $\frac{dA_3}{A_3} = -d\varepsilon_3$ and (a.5.) and (a.6.), we can write:

$$d\bar{\varepsilon} = \frac{2 * I}{i+1} * \frac{dA_3}{A_3}, \quad \bar{\varepsilon} = \frac{2 * I}{i+1} * \ln \frac{A_3}{A_{03}} \qquad (a.14.)$$

where A_{03} is the original surface of A_3.
The work done per unit volume is given by the expression (using the constitutive equation assumed):

$$dW_s = \bar{\sigma} * d\bar{\varepsilon} = K * \bar{\varepsilon}^n * \dot{\bar{\varepsilon}}^m * h(T) * d\bar{\varepsilon} \qquad (a.15.)$$

Keeping in mind that $\dot{\bar{\varepsilon}} = \frac{d\bar{\varepsilon}}{dt}$ and using (a.14.), (a.15.) can be written as:

$$\frac{dW_s}{dA_3} = K * \left(\frac{2 * I}{1+i}\right)^{n+m+1} * \frac{1}{A_3^{m+1}} * \left(\ln \frac{A_3}{A_{03}}\right)^n * \left(\frac{dA_3}{dt}\right)^m * h(T) \qquad (a.16.)$$

Local instability occurs when $\frac{d}{dA_3}\left(\frac{dW_s}{dA_3}\right) = 0$ or:

$$K * \left(\frac{2 * I}{1 + i}\right)^{n+m+1} * \left(\frac{dA_3}{dt}\right)^{m} * \left[\frac{-(m+1)}{A_3^{\,m+2}} * \left(\ln \frac{A_3}{A_{03}}\right)^{n} * h(T) + \right.$$

$$\left. + \frac{n}{A_3^{\,m+2}} \left(\ln \frac{A_3}{A_{03}}\right)^{n-1} * h(T) + \frac{1}{A_3^{\,m+1}} \left(\ln \frac{A_3}{A_{03}}\right)^{n} * \frac{dh(T)}{dA_3}\right] = 0 \qquad (a.17.)$$

or:

$$-(m+1) * h(T) + n * \left(\ln \frac{A_3}{A_{03}}\right)^{-1} * h(T) + A_3 * \frac{dh(T)}{dA_3} = 0 \qquad (a.18)$$

With:

$$\frac{A_3}{h(T)} * \frac{dh(T)}{dA_3} = \frac{1}{h(T)} * \frac{dh(T)}{d\bar{\varepsilon}} * \frac{2 * I}{1 + i} =$$

$$= \frac{1}{h(T)} * \frac{dh(T)}{dT} * \frac{dT}{d\bar{\varepsilon}} * \frac{2 * I}{1 + i} = \frac{\partial \bar{\sigma}}{\partial T} * \frac{\alpha}{\rho * c} * \frac{2 * I}{1 + i} \qquad (a.19.)$$

and (a. 14.), (a. 18.) becomes:

$$-(m+1) + \frac{n}{\bar{\varepsilon}_c} * \frac{2 * I}{1 + i} + \frac{\alpha}{\rho * c} * \frac{\partial \bar{\sigma}}{\partial T} * \frac{2 * I}{1 + i} = 0 \qquad (a.20.)$$

Instability will occur when this expression first becomes zero. This leads to the following expression for the critical strain:

$$\bar{\varepsilon}_c = \frac{2 * I}{1 + i} * \frac{n}{(m+1) - \frac{\alpha}{\rho * c} * \frac{\partial \bar{\sigma}}{\partial T} * \frac{2 * I}{1 + i}} \qquad (a.21.)$$

A.3. Thermal instability

With the assumption of $\bar{\sigma} = \bar{\sigma}(\bar{\varepsilon}, \dot{\bar{\varepsilon}}, T)$, we can write:

$$d\bar{\sigma} = \frac{\partial \bar{\sigma}}{\partial \bar{\varepsilon}} * d\bar{\varepsilon} + \frac{\partial \bar{\sigma}}{\partial \dot{\bar{\varepsilon}}} * d\dot{\bar{\varepsilon}} + \frac{\partial \bar{\sigma}}{\partial T} * dT \qquad (a.22.)$$

Thermal instability occurs when $d\sigma_1 = 0$, which is equal to $d\bar{\sigma} = 0$. With (a.11.) and the constitutive equation (see 3.2.), (a.22.) can be rewritten to obtain:

$$\frac{n}{\bar{\varepsilon}} * d\bar{\varepsilon} + \frac{m}{\dot{\bar{\varepsilon}}} * \frac{d\dot{\bar{\varepsilon}}}{d\bar{\varepsilon}} + \frac{\partial \bar{\sigma}}{\partial T} * \frac{\alpha}{\rho * c} = 0 \qquad (a.23.)$$

Thermal instability occurs when (a.23.) first becomes zero, which leads to the following critical strain:

$$\bar{\varepsilon}_c = \frac{n}{-\frac{m}{\dot{\bar{\varepsilon}}} * \frac{d\dot{\bar{\varepsilon}}}{d\bar{\varepsilon}} - \frac{\partial \bar{\sigma}}{\partial T} * \frac{\alpha}{\rho * c}} \qquad (a.24.)$$

With (a.24.), the calculations for the critical FLITE strains are complete.

Waarin zit 't verschil →
met a 7 op dez. 86
nu eigenlijk? Ik
snap trouwens 't verhaal
bovenaan de pagina niet!

Appendix B. Calculation of the Flow Localization Parameters.

To calculate the FLP's, we assume that the deforming material can be divided into two regions: one containing a defect and the other homogeneous. The condition to be met is that the load supported by the two regions remains equal. If we consider the first principal direction to be critical, this condition can be mathematically expressed as:

$$\delta F_1 = \delta(\sigma_1 * A_1) = \sigma_1 * \delta A_1 + \delta\sigma_1 * A_1 = 0 \qquad (b.1.)$$

or, in words, the variation of force (expressed as the product of stress and surface area) must be equal to zero.
Equation (b.1.) can also be written as:

$$\frac{\delta\sigma_1}{\sigma_1} = -\frac{\delta A_1}{A_1} \quad \text{or} \quad \delta \ln \sigma_1 = \delta\varepsilon_1 \qquad (b.2.)$$

With (a.5.) and $\bar{\sigma} = I * \sigma_1$, $\delta\bar{\sigma} = I * \delta\sigma_1$, (b.2.) becomes:

$$\delta \ln \bar{\sigma} = \frac{2 - i}{2 * I} * \delta\bar{\varepsilon} \qquad (b.3.)$$

With help from the constitutive equation assumed, $\delta \ln \bar{\sigma}$ can be written as:

$$\delta \ln \bar{\sigma} = \left(\frac{\partial \ln \bar{\sigma}}{\partial \bar{\varepsilon}}\right) * \delta\bar{\varepsilon} + \left(\frac{\partial \ln \bar{\sigma}}{\partial \dot{\bar{\varepsilon}}}\right) * \delta\dot{\bar{\varepsilon}} + \left(\frac{\partial \ln \bar{\sigma}}{\partial T}\right) * \delta T \qquad (b.4.)$$

With $\delta T = \dfrac{\alpha * \bar{\sigma} * \delta\bar{\varepsilon}}{\rho * c}$, the temperature term in (b.4.) can be expressed as:

$$\left(\frac{\partial \ln \bar{\sigma}}{\partial T}\right) * \delta T = \left(\frac{\partial \bar{\sigma}}{\partial T}\right) * \frac{\delta T}{\bar{\sigma}} = \left(\frac{\partial \bar{\sigma}}{\partial T}\right) * \frac{\alpha * \delta \bar{\varepsilon}}{\rho * c} \qquad (b.5.)$$

If we neglect strain rate effects, we can rewrite (a.13.) to obtain:

$$\left(\frac{\partial \bar{\sigma}}{\partial T}\right) * \frac{\alpha * \delta \bar{\varepsilon}}{\rho * c} = \left(\frac{-n}{\bar{\varepsilon}_c} + \frac{2-i}{2 * I}\right) * \delta \bar{\varepsilon} \qquad (b.6.)$$

We now insert (b.5.), (b.6.) and the constitutive equation in (b.4.), and thereafter (b.4.) in (b.3.), to obtain:

$$\left(\frac{n}{\bar{\varepsilon}_c} - \frac{n}{\bar{\varepsilon}}\right) = \frac{m}{\delta \bar{\varepsilon}} * \frac{\delta \dot{\bar{\varepsilon}}}{\dot{\bar{\varepsilon}}} \qquad (b.7.)$$

And finally, we use the definition of the flow localization parameter, $FLP = \frac{1}{\dot{\bar{\varepsilon}}} * \frac{\delta \dot{\bar{\varepsilon}}}{\delta \bar{\varepsilon}}$, to obtain:

$$FLP = \left(\frac{n}{\bar{\varepsilon}_c} - \frac{n}{\bar{\varepsilon}}\right) \Big/ m \qquad (b.8.)$$

This is the FLP belonging to the load instability analysis, since the load instability criterion (a.13.) was used to obtain (b.6.) from (b.5.). To obtain the FLP's for local and thermal instability, respectively, the local and thermal instability criteria must be inserted in (b.5.). For the sake of completeness, the results are given below.

$$\text{Local instability FLP} = \left(\frac{n}{\bar{\varepsilon}_c} - \frac{n}{\bar{\varepsilon}} - \frac{(2*i-1)}{2*I} - \frac{m*(1+i)}{2*I}\right) \Big/ m \qquad (b.9.)$$

$$\text{Thermal instability FLP} = \left(\frac{n}{\bar{\varepsilon}_c} - \frac{n}{\bar{\varepsilon}} + \frac{z - i}{2 * I} \right) \Big/ m \qquad (b.10.)$$

Appendix C. The experiments.

C.1. The high-speed tensile tests.

The high-speed tensile tests were carried out on a Zwick rel type 1852 hydraulic tensile testing machine. For each material, ten tests were carried out. One test was carried out to check the setting of the test parameters on the testing machine, the other nine were used to obtain the experimental data. Typical test results are shown in figs. C.1., C.2. and C.3. The setting of the machine parameters is shown in fig. C.4.
The machine provided the experimental data in terms of stress vs. engineering strain. To obtain natural strain values, the following expression was used:

$$\varepsilon = \ln(1 + A) \qquad (C.1.)$$

where ε is natural strain and A is engineering strain.
As mentioned in chapter 4, ε_{cexp} was taken from the maximum in the stress-strain curves. The corresponding engineering strain is A_g. The fracture strains were determined by measurements, and not by changing the value A from the experimental strains into the corresponding natural strain.

C.2. $\frac{\partial \sigma}{\partial T}$ for PVC and PC.

$\frac{\partial \sigma}{\partial T}$'s for PVC and PC were obtained on the same tensile testing machine that was used for the tensile tests. This was done by using a specially outfitted chamber fit for experiments over a wide temperature range that comes with the machine. The tensile test bars were put inside this chamber and heated to preset temperatures. They were then tensile tested at these temperatures. Since $\frac{\partial \sigma}{\partial T}$ is, to a first approximation, a constant,

Sample-#	INT>Rm Nm	INT>Rb Nm	Rm N/mm2	Rb N/mm2	Ag %	A %	EMOD kN/mm2
2	154.69	199.5	343.8	253.1	22.2	28.0	2.500

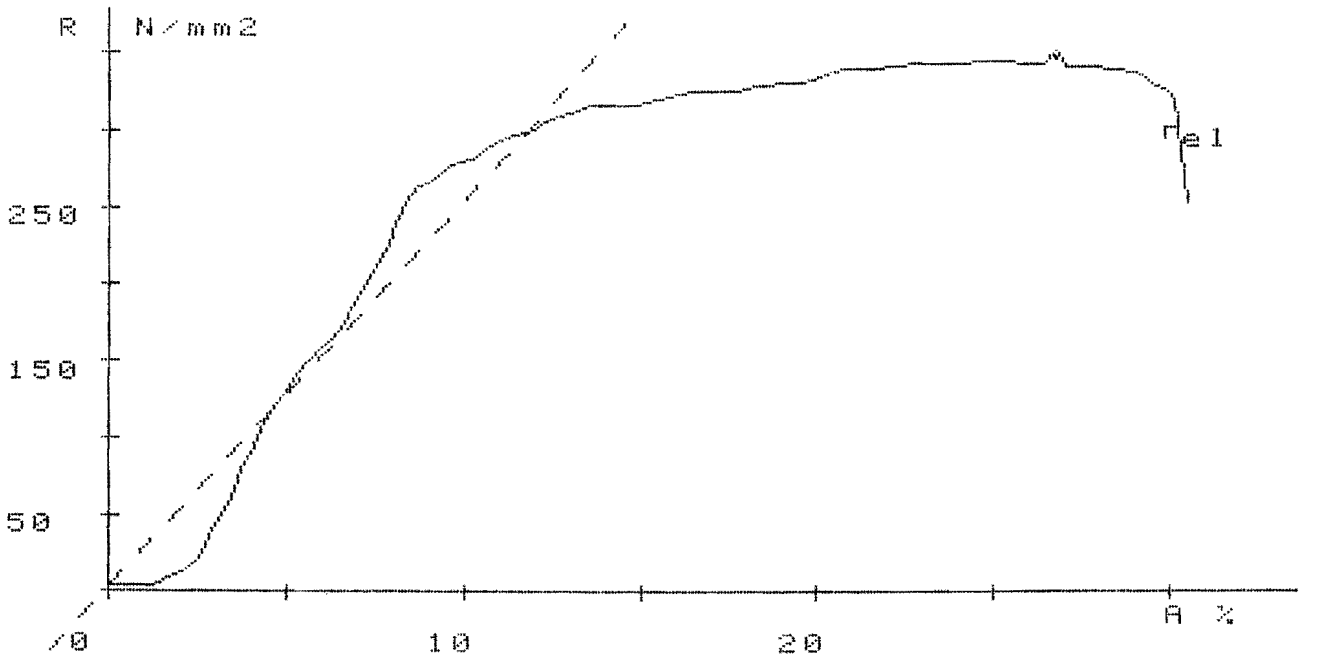

Fig. 1. A typical Al Si St tensile test stress-strain curve.

Sample-#	INT>Rm Nm	INT>Rb Nm	Rm N/mm2	Rb N/mm2	Ag %	A %	EMOD kN/mm2
9	7.16	30.4	84.4	59.2	7.8	28.1	1.428

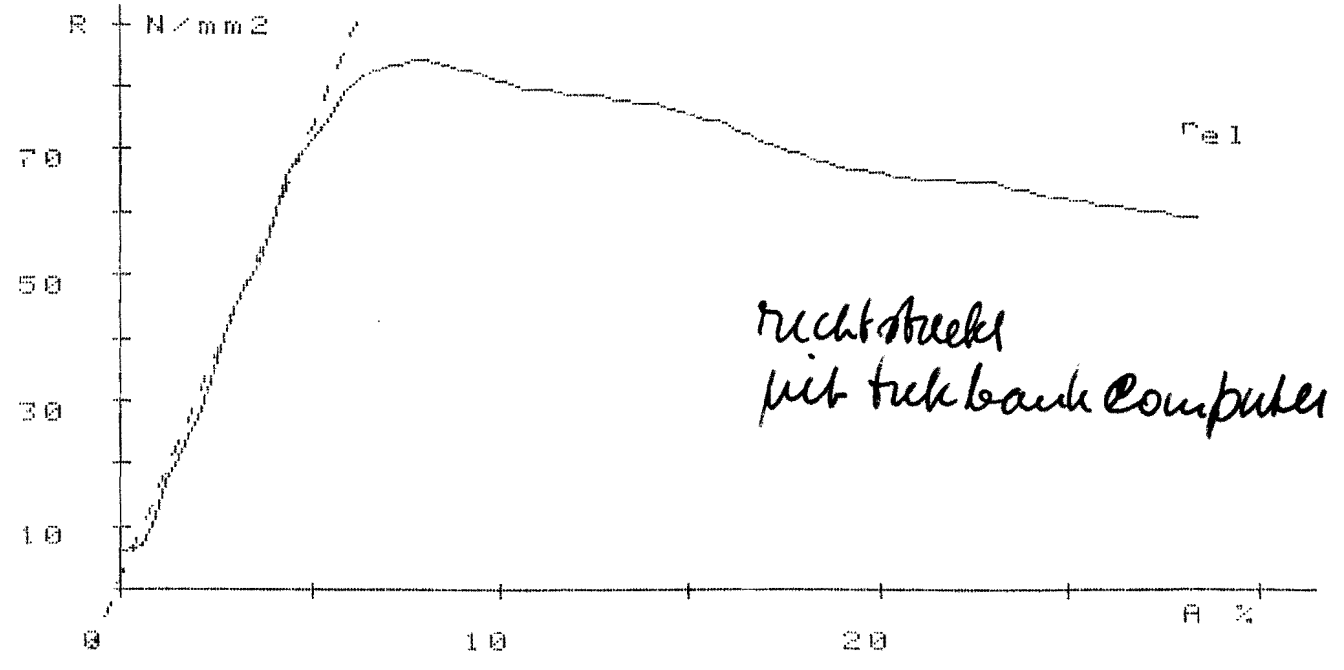

nicht gebrochen
mit Taschenrechner

Fig. 2. A typical PVC tensile test stress-strain curve.

Sample-#	INT>Rm Nm	INT>Rb Nm	Rm N/mm2	Rb N/mm2	Ag %	A %	EMOD kN/mm2
6	6.45	113.3	61.2	43.1	9.8	138.7	0.847

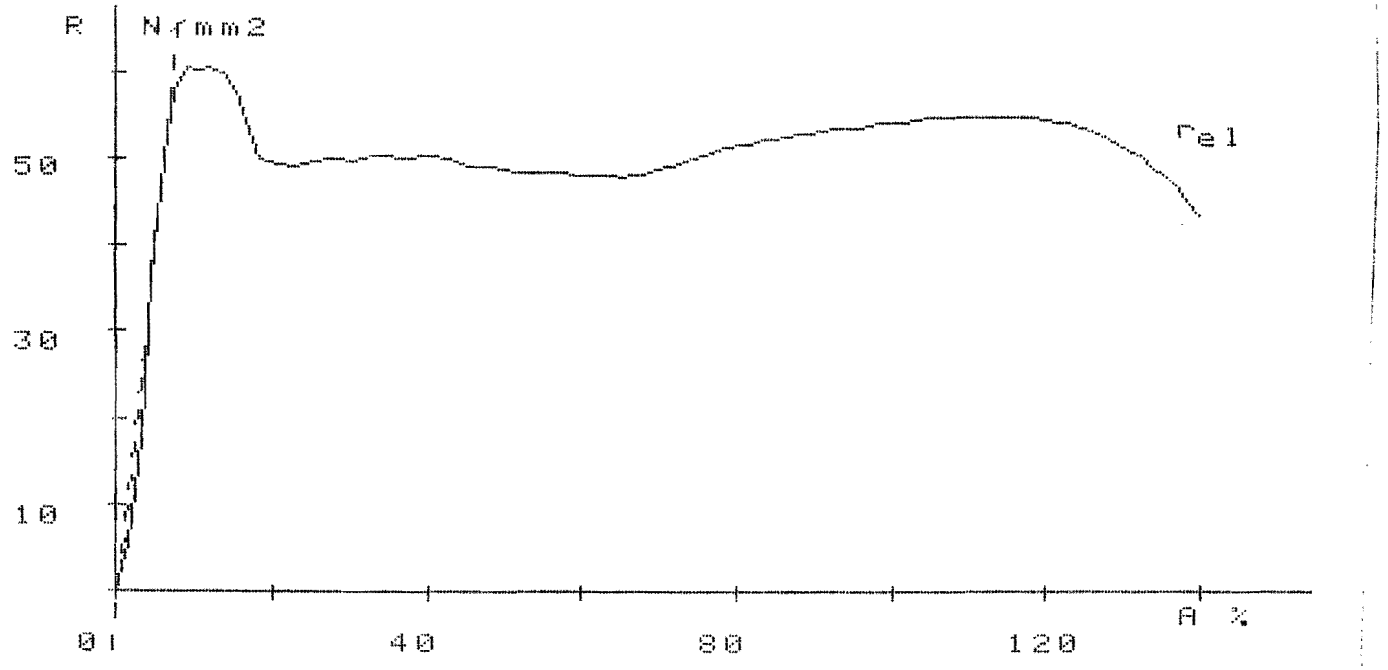

Fig. 3. A typical PC tensile test stress-strain curve.

Int > Rm = deformation work done up to the tensile strength.

Int > Rb = deformation work done up to fracture (total deformation work).

Rm = tensile strength.

Rb = fracture stress.

Ag = maximum homogeneous engineering strain

A = total engineering strain

EMOD = Young's modulus

a straight line was calculated to fit the values of the tensile strength at the lowest and highest test temperatures. The slope of this line is the value of $\frac{\partial \sigma}{\partial T}$. The results can be found in table C.1.

DIALOG-CONTROL: 1 PROTOCOL-CONTROL: 4

FIELD-No	Shortname:	Standard-Text
1	Record-N	
2	Serie	
3	Ordre	
4	Material	
5	Remarks	
6	Date	
7	Test-Engin	
8	Groep	
9	Coach	
10		

THE/TOK
PC/TROUIDUR // Al 51 ST

14-9-1987
J. Boekholt

Fig. 4. The machine parameters.

FIELD-No	Shortname:	Min-Value	Nom-Value	Max-Value	
1	Samole-#	0		1000	
2	Form	1	DIN	4	
3	V-high	0	6 // 1	12	mm/sec
4	V-low	0	0	30000	%/min
5	Grips	0	1.5	1000	N
6	dF-Break	30	80	90	%Fmax
7	Interval	0	10 // 40	99999	msec
8	Delay	0	128	2048	
9	Outp.Modes	10	120	321	
20	DLmaxv	1	40 // 20	200	mm
21	Dv1	0	10	1000	%
22	Dv2	0	20	1000	%
23	Dv3	0	50	1000	%
24	Rmax_v	10	80 // 400	20000	N/mm2
25	Rv1	0	10	20000	N/mm2
26	Rv2	0	20	20000	N/mm2
27	Rv3	0	50	20000	N/mm2
28	F-Channel	0	1	20000	
29	L-Channel	0	3	5	
30	Temp.	-60	21	150	Grd.C
31	Res #31	0	0	0	dim #31
	Res #32	0	0	0	dim #32
	Res #33	0	0	0	dim #33
41	Le	30	100 // 80	500	mm
42	LO	10	60 // 60	500	mm
46	DO	0	—	20	mm
47	DO	0	12,7 // 10	20	mm
52	HO	0	2,1 // 5	5	mm
59	GO	1		100	mm2
60	EMOD	.1		10	kN/mm2
61	Reh	0		20000	N/mm2
62	Rel	0		20000	N/mm2
63	Rm	0		20000	N/mm2
64	Rb	0		20000	N/mm2
65	Ag	0		1000	%
66	A	0		1000	%
67	R1>Dv1	0		20000	N/mm2
68	R2>Dv2	0		20000	N/mm2
69	R3>Dv3	0		20000	N/mm2
70	Es1	0		10	kN/mm2
71	Es2	0		10	kN/mm2
72	Es3	0		10	kN/mm2
73	E1>Rv1	0		100	%
74	E2>Rv2	0		100	%
75	E3>Rv3	0		100	%
76	TUT:Ac	0		4000	Nm
77	TUT:Rm	0		4000	Nm
78	TUT:Rb	0		4000	Nm
79	V-Clamp	0		.5	m/sec
80	Res #80	0		0	dim #80
81	Res #81	0		0	dim #81
82	Res #82	0		0	dim #82
83	Res #83	0		0	dim #83
84	Res #84	0		0	dim #84
85	Res #85	0		0	dim #85

VOORAF IN TE GEVEN WAARDEN

Material	Test temperature [°C]	R_m [N mm^{-2}]	$\frac{\partial \sigma}{\partial T}$ [N mm^{-2} K^{-1}]
PVC	30	63	−0,7
PVC	70	34	
PC	30	63	−0,3
PC	70	51	

Table C.1. Experimental values of $\frac{\partial \sigma}{\partial T}$. R_m is tensile strength.

Finally, tables C.2. and C.3. contain the material parameters obtained from [3] and [9].

Material	ρ [kg mm^{-3}]	c [m] kg^{-1} K^{-1}]	n [-]	$\frac{\partial \sigma}{\partial T}$ [N mm^{-2} K^{-1}]
Ti 6Al-4V	$4{,}43 \cdot 10^{-6}$	$9{,}65 \cdot 10^{5}$	0,07	−1,2

Table C.2. Material parameters from [3]

Material	ρ (lb ft^{-3})	c (Btu °F^{-1} lb^{-1})	n [-]	$\frac{\partial \sigma}{\partial T}$ (psi °F^{-1})
Al 6061 - T6	169	.23	.10	−40
Ti	283	.13	.17	−68

Table C.3. Material parameters from [9]

To obtain the correct dimensions from the material parameters in table C.3. in S.I. units, multiply ρ by 4.978 and leave the other values unchanged.

hoe ziet de →
situatieschets
hierbij eruit?

Appendix D. Metallurgical aspects of FLITE.

There is still much uncertainty about the metallographic nature of the bands of extremely localized deformation often accompanying FLITE. For example, there is still no agreement about the structure of the white bands observed during high-speed punching of steel by Zener and Hollomon (fig. 1., [8]).

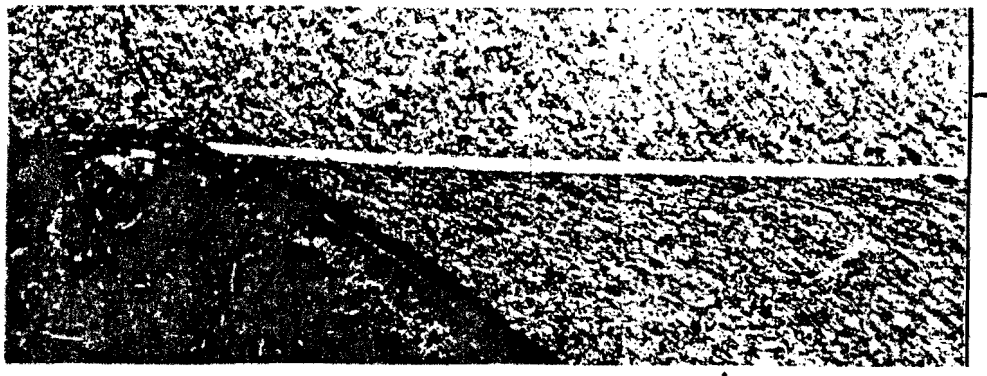

Fig. 1. White band separating the plug from the base material in high-speed punching of steel [8].

It is frequently assumed that these bands, which very often accompany FLITE in steels, are martensitic, but it has also been suggested that they consist of extremely fine-grained, heavily deformed ferrite, or bainite. As pointed out by Bedford et al. [31], this uncertainty will remain until the difficulties associated with physical examination of the bands are removed.

A new approach to the localized band problem has recently been suggested by Timothy [17]. Usually, the bands are called transformed or deformed, depending on whether a phase transformation has occurred in them or not. Timothy suggests that a better analysis of the bands is possible if they are called transformed or deformed according to the partitioning of the prior shear deformation between two zones in metallographic section (fig. 2, 3).

Since the bands occur under a wide variety of conditions, Timothy observes that general observations about them can only be

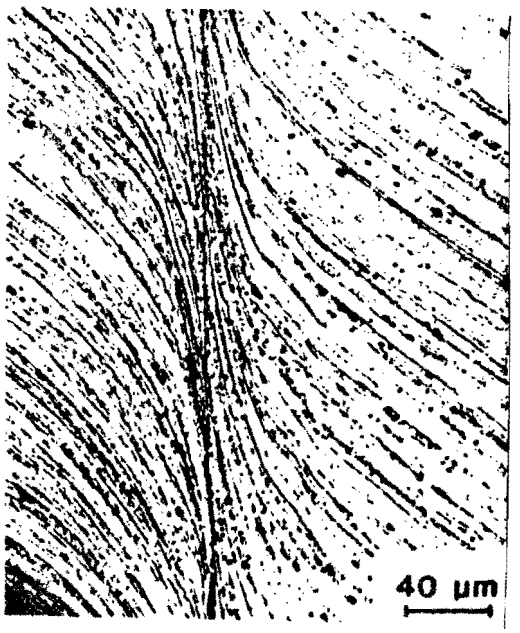

Fig. 2. Deformed shear band in Al 7039 [17]

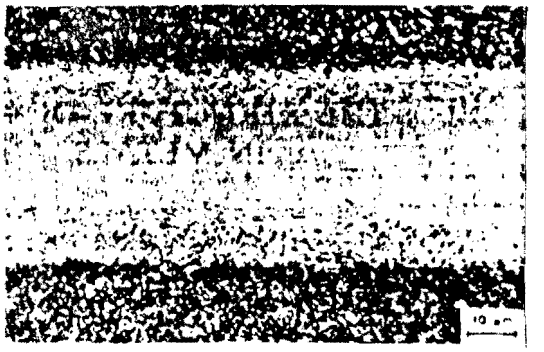

Fig. 3. Transformed shear band in AISI 4340 steel. [17]

qualitative. With this in mind, it can be said that transformed bands are most easily formed in metals of low thermal diffusivity and low resistance to FLITE (high strength, low resistance to flow softening, low rate of strain hardening), like alloy steels and titanium alloys, whereas aluminum and copper tend to form deformed bands. If extreme FLITE occurs, however, transformed bands may eventually appear regardless of the metallurgy of the alloy.

As can be concluded from the above, it is very difficult to interpret data concerning localized deformation bands. It is due to this problem, combined with the limited time available, that no attention has been paid to the metallurgy of FLITE in this report.

Appendix E. FLITE in blanking: an example

In this appendix, an example is given how FLITE theory can be applied to a manufacturing process.
In [47], Ramaekers and Kals derived an expression for the maximum effective strain in the narrowest section s during the punching operation (fig. D. 1.):

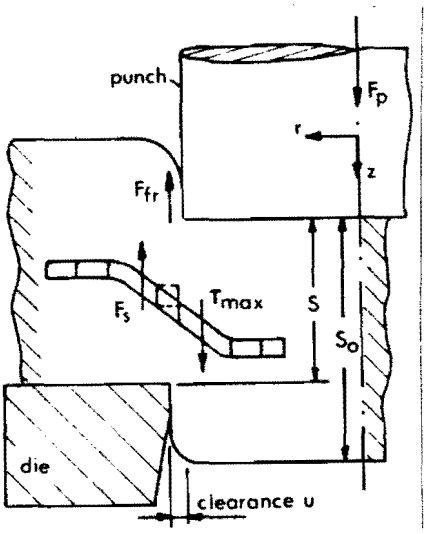

Fig. D. 1. Idealized model of the punching operation [47]

$$\varepsilon = \sqrt{\left(\frac{3}{n}\right)} * \ln \frac{s_o}{s} \qquad (D.\ 1.).$$

This process may be described by using a simple shear model, which means that the stress path i has a value of -1.
Should the maximum strain from (D. 1.) be equal to or larger than the critical FLITE strains, FLITE may occur. This condition leads to a critical narrowest section, which may be expressed as follows:

$$\frac{s_o}{s_c} = \exp\left(\sqrt{\left(\frac{n}{3}\right)} * \varepsilon_{cload}\right) \qquad (D.\ 2.)$$

with s_c the critical narrowest section and ε_{cload} the critical load instability strain (the thermal instability strain can, of course, also be used).
(D. 2.) may be rewritten as follows:

$$s_c = s_0 * \exp - \left(\sqrt{\frac{n}{3}} * \varepsilon_{cload}\right) \qquad (D.3.).$$

As an example, the critical narrowest section for Ti (see chapter 4) would be :

$$s_{cTi} = 0,97 * s_0 \qquad (D.4.).$$

And with the thermal instability strain :

$$s_{cTi} = 0,88 * s_0 \qquad (D.5.).$$

This means that the possibility that FLITE will occur in Ti during punching is high. To determine whether it occurs or not, the FLP must be known. The FLP for punching can be obtained by using (D.2.) as the current strain ε :

$$FLP = \left(\frac{n}{\varepsilon_c} - \frac{n * \sqrt{\left(\frac{n}{3}\right)}}{\ln s_0/s}\right) \Big/ m \qquad (D.6.).$$

For illustrative purposes, a thermal instability FLP will be used (there is no value of the load instability FLP for the onset of noticeable localization). Noticeable localization corresponds to FLP = s, which gives the following s-value :

$$s = 0,81 * s_0 \qquad (D.7.).$$

This means, that during punching of Ti, noticeable localization will occur. Whether this also means that the final product is smooth-sheared must be investigated.
With this example, one of the possible uses of FLITE theory has been demonstrated.